Article:
Shahid, N, Burrows, KE, Pask, CM et al. (2022) Heteroleptic Iron(II) Complexes of Chiral 2,6-Bis(oxazolin-2-yl)pyridine (PyBox) and 2,6-Bis(thiazolin-2-yl)pyridine Ligands – the Interplay of Different Ligands on the Metal Ion Spin State. Dalton Transactions, 51 (11). pp. 4262-4274. ISSN: 1477-9226

https://doi.org/10.1039/D2DT00393G

Heteroleptic Iron(II) Complexes of Chiral 2,6-*Bis*(oxazolin-2-yl)-pyridine (PyBox) and 2,6-*Bis*(thiazolin-2-yl)pyridine Ligands – the Interplay of Two Different Ligands on the Metal Ion Spin State¶†‡

Namrah Shahid,[a,b] Kay E. Burrows,[a] Christopher M. Pask,[a] Oscar Cespedes,[c] Mark J. Howard,[a] Patrick C. McGowan[a] and Malcolm A. Halcrow[a,*]

Complexation of $Fe[ClO_4]_2{\cdot}6H_2O$ by 1 equiv 2,6-*bis*((4*S*)-4-phenyl-4,5-dihydrooxazol-2-yl)pyridine ((*S*)-*L*^{1}Ph) and 2,6-*bis*((4*R*)-4-phenyl-4,5-dihydrothiazol-2-yl)pyridine ((*R*)-*L*^{2}Ph) cleanly affords $[Fe((S)\text{-}L^1Ph)((R)\text{-}L^2Ph)][ClO_4]_2$; $[Fe((R)\text{-}L^1iPr)((S)\text{-}L^2iPr)][ClO_4]_2$ (*L*^{1}*i*Pr = 2,6-*bis*(4-*iso*propyl-4,5-dihydrooxazol-2-yl)pyridine; *L*^{2}*i*Pr = 2,6-*bis*(4-*iso*propyl-4,5-dihydrothiazol-2-yl)pyridine) was prepared by a similar route. The compounds exhibit thermal spin-crossover in solution, at temperatures midway between the corresponding $[Fe((R)\text{-}L^1R)((S)\text{-}L^1R)][ClO_4]_2$ and $[Fe((R)\text{-}L^2R)((S)\text{-}L^2R)][ClO_4]_2$ (R = Ph or *i*Pr) species. The spin states of $[Fe(LR)(bimpy)][ClO_4]_2$ and $[Fe(LR)(bpp)][ClO_4]_2$ (*L*R = *L*^{1}R or *L*^{2}R; bimpy = 2,6-*bis*(1*H*-benz-imidazol-2-yl)pyridine; bpp = 2,6-di(pyrazol-1-yl)pyridine) are also reported, with most examples exhibiting gradual spin-crossover in solution and the solid state. Although some products undergo partial ligand exchange in solution by ^{1}H NMR, their solution $T_{½}$ values appear unaffected by this and correlate well with their spin state energies from gas phase DFT calculations. The high-spin state of $[Fe(L^2R)(bpp)]^{2+}$ is more stabilised than expected, compared to the other $[Fe(LR)L]^{2+}$ complexes studied (L = bimpy, bpp or terpy). That is explained by an interplay between the relative σ-basicities and π-acidities of the two ligands in each molecule. The steric influence of their phenyl or *iso*propyl 'R' substituents stabilises the heteroleptic complexes by up to 5 kcal mol^{-1}, compared to analogues lacking these groups.

Introduction

While the phenomenon was first recognised in the 1960s,[1] spin-crossover (SCO) compounds have attracted special interest during the last thirty years,[2-4] when their potential applications as switching components in memory and display devices were recognised.[5] A variety of macro- and nano-scale applications of SCO materials have since been demonstrated in the laboratory, and are under active development.[6,7] The best studied SCO compounds are molecular complexes, coordination polymers or networks of iron(II) with nitrogen-donor ligands.[8-10] The most common stoichiometries in molecular SCO chemistry are $[FeX_2(NN)_2]$ (X^- = a pseudohalide),[11,12] $[Fe(NN)_3]^{2+}$ [8,13-15] or $[Fe(NNN)_2]^{2+}$,[8,14-19] where NN and NNN represent bidentate and tridentate N-donor ligands. Most $[Fe(NN)_3]^{2+}$ and $[Fe(NNN)_2]^{2+}$ complexes are homoleptic, since attempts to prepare heteroleptic complexes of labile metal ions with different bi- or tridentate ligands, often afford statistical mixtures of products.[20-22] However, heteroleptic SCO complexes of two tridentate ligands based on 2,6-di(1*H*-pyrazol-3-yl)pyridine,[22,23] *tris*(pyrazol-1-yl)methane[24] or anionic Schiff base derivatives[25] can be reliably isolated in pure form. Combining different N-donor ligands about the same metal ion gives added potential to fine-tune the SCO properties of a complex or material.[26]

We, and others, have used chiral 2,6-*bis*(4,5-dihydrooxazol-2-yl)pyridine (PyBox; *L*^{1}R, Scheme 1)[27] and 2,6-*bis*(4,5-dihydrothiazol-2-yl)pyridine (ThioPyBox; *L*^{2}R) ligands to probe the spin states of different diastereomers of $[Fe(L^1R)_2]^{2+}$ and $[Fe(L^2R)_2]^{2+}$ derivatives.[28-30] The comparison was possible because some heterochiral $[Fe((R)\text{-}LR)((S)\text{-}LR)]^{2+}$ (*L*R = *L*^{1}R or *L*^{2}R) complexes are stable to racemisation in solution. That should reflect destabilisation of homochiral $[Fe((R)\text{-}LR)_2]^{2+}$ and $[Fe((S)\text{-}LR)_2]^{2+}$ by steric clashes between their 'R' substituents, which are not present in the heterochiral isomer.[20] DFT calculations confirmed $[Fe((R)\text{-}LR)((S)\text{-}LR)]^{2+}$ have lower energy than the corresponding $[Fe((R)\text{-}LR)_2]^{2+}$ species when R = Ph or *i*Pr.[30]

We reasoned the same steric influence of the peripheral 'R' substituents could stabilise heteroleptic SCO complexes $[Fe(L^1R)L]^{2+}$ or $[Fe(L^2R)L]^{2+}$ (L = another meridional tridentate ligand).[31] The chirality of such compounds is another attractive feature, since chiral-at-molecule SCO complexes are still quite rare.[28-30,32] Such compounds have potential for switchable ferroelectric or chiroptical properties in the solid state.[33,34]

[a] *School of Chemistry, University of Leeds, Woodhouse Lane, Leeds, UK LS2 9JT. E-mail: m.a.halcrow@leeds.ac.uk*

[b] *Current address: Department of Chemistry, University of Durham, Durham, UK DH1 3LE.*

[c] *School of Physics and Astronomy, University of Leeds, WH Bragg Building, Leeds, UK LS2 9JT.*

¶ Dedicated to Paul R. Raithby, celebrating a career in inorganic and organometallic chemistry, on the occasion of his 70th birthday.

† Data supporting this study are available at http://doi.org/10.5518/###

‡ Electronic Supplementary Information (ESI) available: synthetic protocols and characterisation data for the complexes in this work; experimental data, refinement details, figures and tables for the crystal structure determinations; additional solid and solution phase characterisation data; and details of the minimised structures from the DFT calculations. CCDC 2132824–2132830 and 2134550. For ESI and crystallographic data in CIF or other electronic format see DOI: 10.1039/x0xx00000x

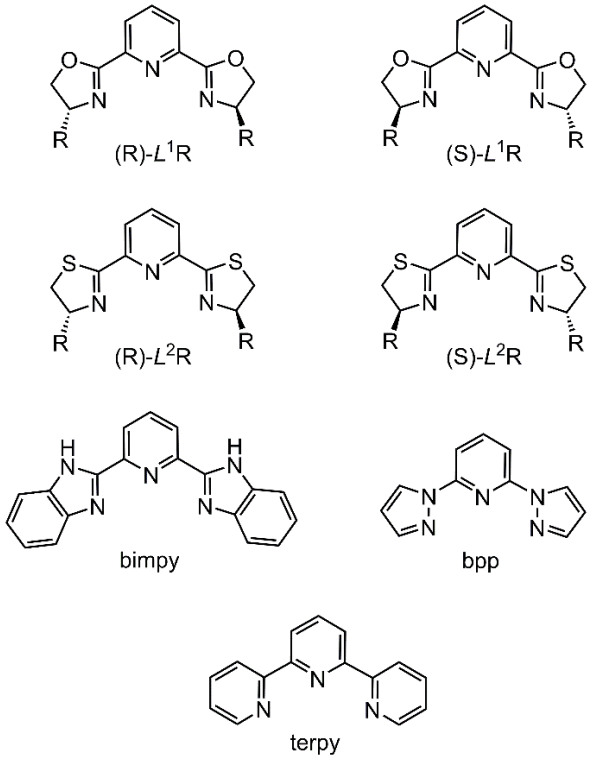

Scheme 1 The ligands used in this study (R = Ph or *i*Pr).

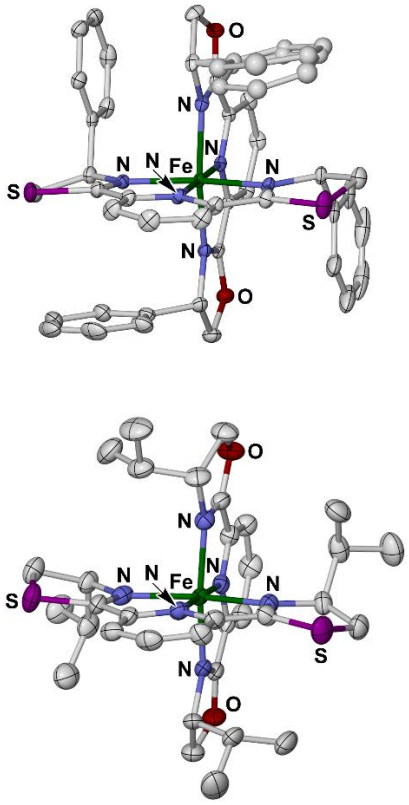

Figure 1 The complex cation in **1**·$MeNO_2$ (top), and molecule A in **2**·MeCN (bottom).[37] Both orientations of a disordered phenyl ring in **1**·$MeNO_2$ are included. Displacement ellipsoids are at the 50 % probability level, and H atoms have been removed for clarity. Colour code: C, white; Fe, green; N, blue; O, red; S, purple.

This report describes our efforts towards that end. First, are two heterochiral complexes $[Fe(L^1R)(L^2R)]^{2+}$ (R = Ph or *i*Pr), containing L^1R and L^2R ligands of opposite handedness. Second, is a wider investigation of $[Fe(L^1R)L]^{2+}$ or $[Fe(L^2R)L]^{2+}$ complexes containing three other 'L' co-ligands (Scheme 1).[35,36]

Results and Discussion

Reaction of (*S*)-L^1Ph and (*R*)-L^2Ph with $Fe[ClO_4]_2{\cdot}6H_2O$ in a 1:1:1 mole ratio in acetonitrile yielded a dark purple solution, which gave a purple solid product following the usual work-up.[37] Recrystallisation of this material from nitromethane/diethyl ether afforded crystals of $[Fe((S)\text{-}L^1Ph)((R)\text{-}L^2Ph)][ClO_4]_2{\cdot}MeNO_2$ (**1**·$MeNO_2$), which retain their lattice solvent by microanalysis. The complex $[Fe((R)\text{-}L^1iPr)((S)\text{-}L^2iPr)][ClO_4]_2$ (**2**) was prepared similarly, but gave single crystals directly from the acetonitrile reaction mixture. These crystals have formula **2**·MeCN, but decompose to the solvent-free material on exposure to air. While both complexes are heterochiral diastereomers, the L^1R and L^2R ligands in **1** and **2** have opposite handedness.[37]

Crystallographic characterisation of solvate crystals of **1** and **2** confirmed their heteroleptic formulations (Figure 1); there is no evidence for disorder of the O and S atom sites in either analysis. Both **1** and **2** are low-spin at the temperature of measurement, which is consistent with the magnetic properties described below (Table S2). Their ligand conformations resemble those in low-spin, heterochiral $[Fe(L^1Ph)_2][ClO_4]_2$,[28,29] $[Fe(L^2Ph)_2][ClO_4]_2$ and $[Fe(L^2iPr)_2][ClO_4]_2$[30] (Figure 1). The more puckered conformation of the thiazoline rings in the L^2R ligands, compared to the oxazoline rings in L^1R, is particularly clear.

Samples of **1**·$MeNO_2$ are crystalline and phase-pure by powder diffraction, but loss of solvent from **2** yields a poorly crystalline solid, with a significant fraction of amorphous material (Figure S4‡). Magnetic susceptibility data show that **1**·$MeNO_2$ is low-spin in the solid state between 5-350 K (Figure S5‡). That is unsurprising, since its homoleptic congeners $[Fe((R)\text{-}L^1Ph)((S)\text{-}L^1Ph)][ClO_4]_2$ and $[Fe((R)\text{-}L^2Ph)((S)\text{-}L^2Ph)][ClO_4]_2$ are also low-spin.[28-30] More informative is **2** which exhibits an SCO equilibrium on cooling. This is centred near room temperature but is very gradual and incomplete, reflecting the poor crystallinity of the sample (Figure S5‡). In comparison, solid $[Fe((R)\text{-}L^1iPr)((S)\text{-}L^1iPr)][ClO_4]_2$ is high-spin at all temperatures, while $[Fe((R)\text{-}L^2iPr)((S)\text{-}L^2iPr)][ClO_4]_2$ is low-spin at room temperature and exhibits SCO with $T_{½} > 400$ K.[28,30] Hence, the spin state properties of **2** lie between the homoleptic complexes of its constituent ligands.

Freshly mixed solutions of a 1:1:1 ratio of (*S*)-L^1Ph, (*R*)-L^2Ph and $Fe[ClO_4]_2{\cdot}6H_2O$ in CD_3CN contain an approximate statistical mixture of $[Fe((S)\text{-}L^1Ph)_2]^{2+}$, $[Fe((R)\text{-}L^2Ph)_2]^{2+}$ and $[Fe((S)\text{-}L^1Ph)((R)\text{-}L^2Ph)]^{2+}$ (**1**) by ^{1}H NMR (Figure 2). The fraction of heteroleptic **1** in the solution increases on standing, until the mixture reaches a constant composition after *ca* 3 days. Complex **1** is the main component of the mixture after equilibration, although *ca* 15 % of the iron content is residual homochiral $[Fe((S)\text{-}L^1Ph)_2]^{2+}$ (Figure 2). Similar results were obtained from an analogous measurement of the formation of **2**, although equilibration of that solution occurred within 1 hour

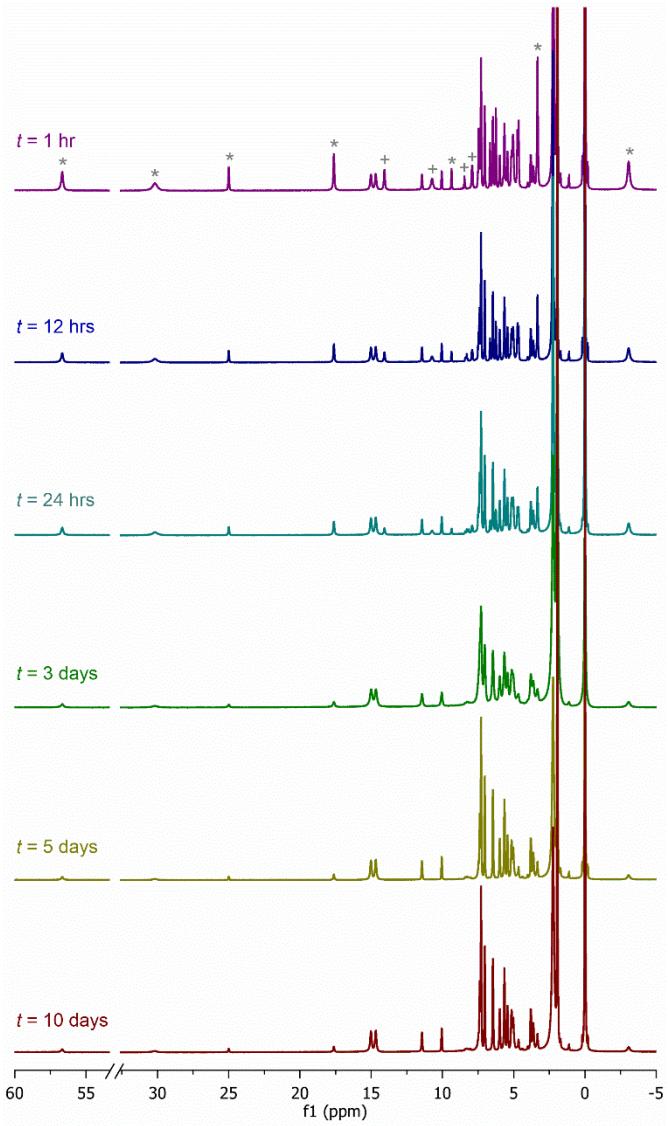

Figure 2 ^{1}H NMR spectra of a 1:1:1 mixture of (*S*)-*L*^{1}Ph, (*R*)-*L*^{2}Ph and $Fe[ClO_4]_2{\cdot}6H_2O$ in CD_3CN solution. Peaks from $[Fe((S)\text{-}L^1Ph)_2]^{2+}$ are starred,[28] and peaks from $[Fe((R)\text{-}L^2Ph)_2]^{2+}$ are marked with a cross (other peaks in the diamagnetic region are also from this species).[30] An expansion of a fully equilibrated spectrum is shown in Figure S6‡.

(Figure S7‡). That probably reflects the larger population of the more labile high-spin state in the components of that solution.

The NMR spectra of preformed **1** and **2** in CD_3CN resemble these equilibrated spectra, with the same ligand exchange byproducts being present (Figures S6-S7‡). The solution speciation of **2** resembles $[Fe((R)\text{-}L^1iPr)((S)\text{-}L^1iPr)]^{2+}$, which is also high-spin at room temperature.[28] Ligand exchange in **1** was unexpected however, since homoleptic $[Fe((R)\text{-}LPh)((S)\text{-}LPh)]^{2+}$ (*L*Ph = *L*^{1}Ph or *L*^{2}Ph) are both stable in solution by NMR.[28,30]

Magnetic measurements from **1** and **2** in CD_3CN in solution show partial SCO over the liquid range of the solvent, which yield typical thermodynamic parameters for iron(II) SCO when modelled as a single equilibrium (Figure 3, Table 1). A low-temperature paramagnetic impurity of 0.25 cm^3 mol^{-1} K was included in the fit for **2**, to account for the partial ligand exchange detected by NMR, but the effect of this correction on

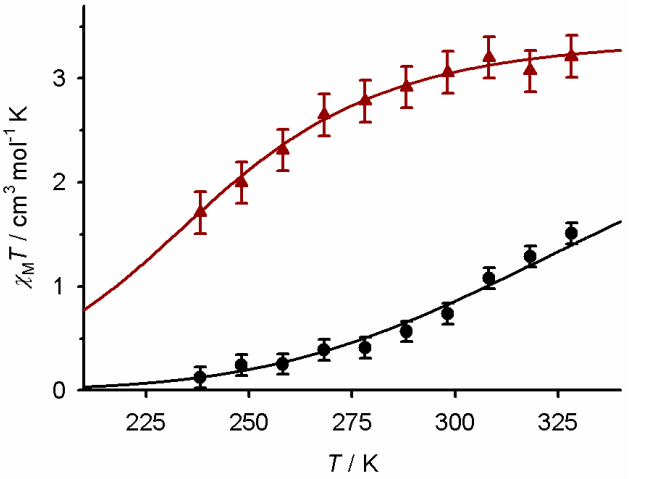

Figure 3 Magnetic data in CD_3CN solution for **1** (black circles) and **2** (red triangles). The lines show the best fits of these data to a thermodynamic SCO equilibrium (see the Experimental section).

Table 1 Solution SCO parameters for the compounds in this work, measured in CD_3CN. Data for the homoleptic analogues of **1** and **2** are also included, for comparison.[a]

	$T_{½}$ / K	ΔH / kJ mol^{-1}	ΔS / J mol^{-1} K^{-1}
$[Fe((R)\text{-}L^1Ph)((S)\text{-}L^1Ph)][ClO_4]_2$[28]	278 ±2	26.2	94
1	344 ±5	21.1 ±1.2	61 ±5
$[Fe((R)\text{-}L^2Ph)((S)\text{-}L^2Ph)][ClO_4]_2$[30]	LS	–	–
$[Fe((R)\text{-}L^1iPr)((S)\text{-}L^1iPr)][ClO_4]_2$[28]	HS	–	–
2[b]	241 ±3	21.2 ±1.5	88 ±7
$[Fe((R)\text{-}L^2iPr)((S)\text{-}L^2iPr)][ClO_4]_2$[30]	LS	–	–
3	292 ±1	21.7 ±0.6	74 ±2
4	>380	–	–
5[c]	221 ±12	20 ±5	89 ±27
6	330 ±1	21.2 ±0.4	64 ±2
7	285 ±1	20.3 ±0.6	71 ±3
8[b]	364 ±3	22.0 ±0.5	60 ±2
9[b]	232 ±4	24 ±2	104 ±10
10[c]	266 ±2	23.9 ±1.8	90 ±7

[a]HS = high-spin, LS = low-spin over the liquid range of the solvent. [b]Fit assuming a residual low-temperature $\chi_M T$ value of 0.25 cm^3 mol^{-1} K. [c]Fit assuming a residual low-temperature $\chi_M T$ value of 0.50 cm^3 mol^{-1} K.

the fitted parameters lies inside their experimental error. No such correction was required for **1**, since its homochiral impurities are themselves low-spin at low temperature.[28,29] Although the solution ligand exchange means their errors may be under-estimated, the $T_{½}$ values derived from these fits are supported by the DFT calculations described below.

Other heteroleptic complexes were pursued by complexing $Fe[ClO_4]_2{\cdot}6H_2O$ with equimolar amounts of either *L*^{1}R or *L*^{2}R, and another tridentate N-donor ligand. This yielded purple $[Fe(LR)(bimpy)][ClO_4]_2$ (*LR* = (*R*)-*L*^{1}Ph, **3**; *LR* = (*R*)-*L*^{2}Ph, **4**; *LR* = (*S*)-*L*^{1}*i*Pr, **5**; *LR* = (*S*)-*L*^{2}*i*Pr, **6**), and red or brown $[Fe(LR)(bpp)][ClO_4]_2$ (*LR* = (*R*)-*L*^{1}Ph, **7**; *LR* = (*R*)-*L*^{2}Ph, **8**; *LR* = (*S*)-*L*^{1}*i*Pr, **9**; *LR* = (*S*)-*L*^{2}*i*Pr, **10**).[37] While samples of **3**-**6** were visually homogeneous, freshly crystallised **7**-**10** were often contaminated by yellow crystals of

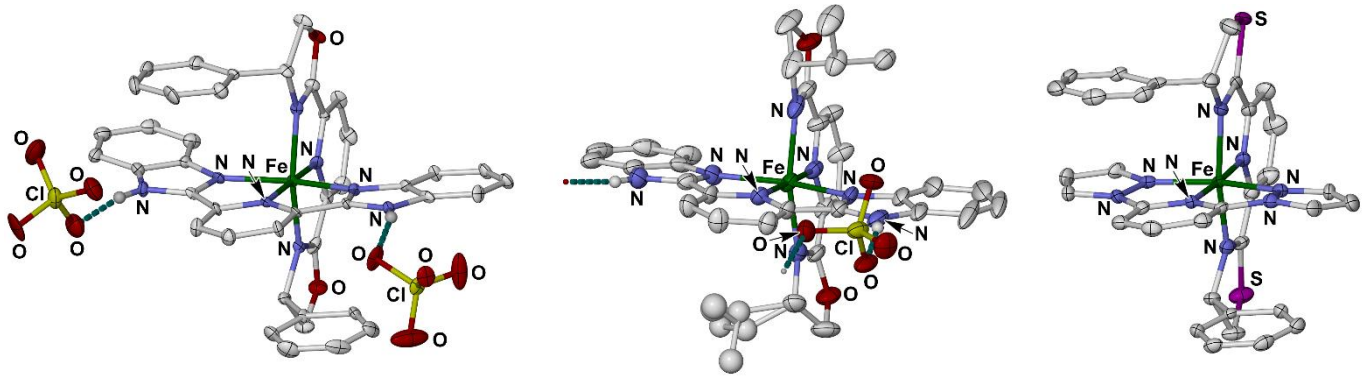

Figure 4 A $[Fe((R)\text{-}L^1Ph)(bimpy)][ClO_4]_2$ assembly in **3**·MeCN (molecule A, left); the $\{[Fe((S)\text{-}L^1iPr)(bimpy)](\mu\text{-}ClO_4)\}^+$ hydrogen-bonding motif in **5** (centre); and the $[Fe((R)\text{-}L^2Ph)(bpp)]^{2+}$ molecule in **8**·2MeCN (right). Both orientations of a disordered *iso*propyl group in **5** are shown. Displacement ellipsoids are at the 50 % probability level, and *C*-bound H atoms have been removed for clarity. Colour code: C, white; Cl, yellow; Fe, green; N, blue; O, red; S, purple.

$[Fe(bpp)_2][ClO_4]_2$.[38] That impurity was removed manually to afford pure samples for characterisation. All these compounds were obtained in analytical purity, with some containing lattice solvent whose presence was often confirmed crystallographically.

Dark purple solids analysing as $[Fe(\mathit{L}R)(terpy)][ClO_4]_2$ ($\mathit{L}R$ = (R)-L^1Ph, **11**; $\mathit{L}R$ = (S)-L^1*i*Pr, **12**) were obtained from extended complexation reactions using terpy as co-ligand. However, recrystallised samples derived from these materials always contained $[Fe(terpy)_2][ClO_4]_2$,[39] as the only crystalline product. Unlike **7**-**10**, the dark colours and similar appearance of $[Fe(\mathit{L}^1R)(terpy)][ClO_4]_2$, $[Fe(\mathit{L}^1R)_2][ClO_4]_2$[28,29] and $[Fe(terpy)_2][ClO_4]_2$[39] made it challenging to perform a Pasteur purification on **11** and **12**. Hence, the detailed characterisation of those compounds was not pursued.[40]

Structure refinements from crystals of **3**-**6** were obtained at a temperature between 100-130 K (Figures 4 and S8-S11‡). The structures show **3**·MeCN, **4** and **6**·MeCN·Et_2O are low-spin under those conditions, but **5** adopts a mixed high:low-spin population at that temperature (Table S3‡). That is consistent with the magnetic data for **5**, as described below (Figure 5, top). The bimpy ligand in **4** has an S-shaped conformation, reflecting an intermolecular steric clash at one of its benzimidazolyl residues (Figure S13‡). That has no effect on the inner coordination sphere of the molecule however, whose metric parameters resemble the other low-spin compounds in this study. The only molecule whose structure appears to be influenced by intramolecular steric interactions is **5**, whose bimpy ligand is canted by 5.92(9)° from perpendicular with respect to the L^1*i*Pr ligand N-donor atoms (Table S3‡). The canting reflects the positioning of the *iso*propyl substituents above and below the bimpy ligand, and may contribute to stabilising the high-spin state of that complex.

The bimpy ligands donate N–H···O hydrogen bonds to the ClO_4^- ions or, in one case, to a diethyl ether solvent molecule. These interactions afford discrete $\{[Fe(\mathit{L}R)(bimpy)][ClO_4]_2\}$ or $\{[Fe(\mathit{L}R)(bimpy)][ClO_4][solvent]\}^+$ assemblies in **3**·MeCN, **4** and **6**·MeCN·Et_2O. However, the cations in **5** donate two hydrogen bonds to the same anion, giving $\{[Fe(\mathit{L}^1iPr)(bimpy)][\mu\text{-}ClO_4]\}^+$ hydrogen-bonded chains zig-zagging along the [100] vector.

Solid **3**·MeCN retains its lattice solvent by microanalysis on exposure to air, while the analysis of **4** is best fit by the formulation **4**·H_2O despite its single crystals being solvent-free. Dried samples of **5** and **6** analyse as solvent-free materials. X-ray powder diffraction data for **3**·MeCN-**5** show good agreement with their crystallographic simulations, but **6**·MeCN·Et_2O transforms to a new polycrystalline phase during loss of its lattice solvent upon exposure to air (Figure S14‡).

Magnetic susceptibility data show **3**·MeCN exhibits a gradual SCO equilibrium with $T_{½}$ = 340 ±5 K, which is reversible above room temperature and so is not associated with loss of lattice solvent (Figure 5, top).[41] The equilibrium is complete around 170 K, and the material is fully low-spin below that temperature.

Solid **5** is predominantly high-spin at room temperature ($\chi_M T$ = 2.8 cm^3 mol^{-1} K at 300 K), and exhibits gradual and incomplete SCO on cooling (Figure 5, top). The SCO midpoint temperature can be estimated at $T_{½}$ = 150 ±10 K, but around 40 % of the sample remains high-spin at 80 K, and is kinetically trapped in that form below that temperature.[42] Conversely, **4**·H_2O and **6** are low-spin between 5-370 K, although **4**·H_2O shows a small irreversible increase in $x_M T$ above room temperature that could be associated with loss of its lattice water on heating. All these magnetic data are consistent with the spin states in the crystal structures of the compounds.

^{1}H NMR spectra of the preformed complexes in CD_3CN show **3**, **4** and **6** are stable in that solvent (Figures S15-S18‡). However, the spectrum of **5** contains some $[Fe((S)\text{-}L^1iPr)_2]^{2+}$ as a minor contaminent,[28] along with a diamagnetic species that could be metal-free bimpy (Figure S17‡). Hence, that complex undergoes some ligand redistribution in solution, which might be a consequence of the greater steric influence of its *i*Pr substituents. Alternatively, it could simply reflect that **5** adopts the labile high-spin state at room temperature in that solvent, whereas the solutions of **3**, **4** and **6** contain differing fractions of their more inert low-spin form (Figure 5, bottom). These spectra were all unchanged after standing for 24 hrs.

All four complexes exhibit SCO in CD_3CN, although the onset of SCO for **4** is only just evident at the highest temperature of the measurement. Their $T_{½}$ values follow the trend (Table 1):

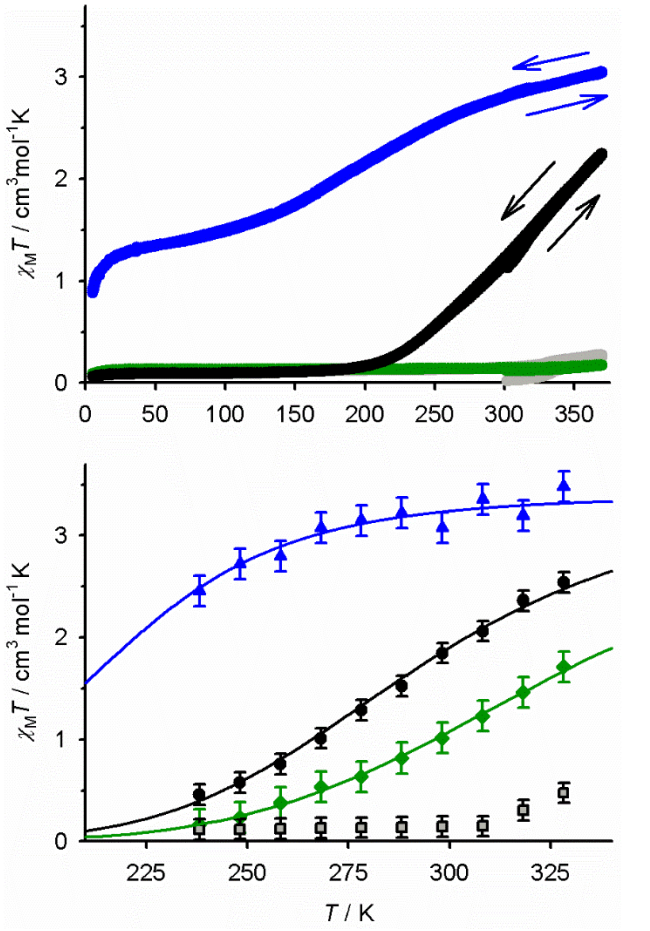

Figure 5 Magnetic data for **3**·MeCN (black circles), **4**·H_2O (grey squares), **5** (blue triangles) and **6** (green diamonds). Top; solid state data, measured on a 300⟶370⟶5⟶300 K temperature cycle at a scan rate 5 K min^{-1}. Bottom; data in CD_3CN solution. The lines show the best fits of the solution data for **3**, **5** and **6** to a thermodynamic SCO equilibrium. A residual low-temperature $\chi_M T$ = 0.50 $cm^3 mol^{-1}$ K value was included in the fit for **5**, to account for the partial ligand exchange in its solution.

5 (*L*R = L^1*i*Pr) < **3** (L^1Ph) < **6** (L^2*i*Pr) < **4** (L^2Ph)

which is consistent with their solid state magnetic data. A low-temperature paramagnetic impurity of 0.50 cm^3 mol^{-1} K was included in the fit for **5**, reflecting the significant ligand exchange detected by NMR for that compound.

Only one bpp complex formed crystals suitable for X-ray diffraction, namely **8**·2MeCN (Figure 4). This is also low-spin at 120 K, and has comparable metric parameters to the bimpy complexes (Table S6). Solid **8**·MeCN·H_2O (the analytical formulation of that compound) is moderately crystalline, and is low-spin between 5-370 K (Figures S21-S22‡). The other bpp complexes are poorly crystalline by powder diffraction. Samples of **7** show a gradual and incomplete thermal SCO with $T_{½}$ = 275 ±5 K, which is *ca* 85 % complete after the onset of thermal trapping below 80 K[42] and has a mixed-spin population at 300 K ($\chi_M T$ = 2.2 cm^3 mol^{-1} K). **10**·2H_2O behaves similarly, but its SCO is more gradual so *ca* 40 % of that compound remains high-spin below 80 K. Lastly, **9**·$MeNO_2$ is high-spin at 300 K, with *ca* 25 % of the material having undergone SCO after cooling to 80 K. Magnetic data from **8**·MeCN·H_2O and **10**·2H_2O both show small, irreversible changes after heating to 370 K, implying their spin states are perturbed by loss of lattice solvent (Figure S22).[41]

The only bpp complex that is completely stable by ^{1}H NMR in CD_3CN is **7**. Solutions of **8**-**10** reproducibly contain detectable quantities of $[Fe(bpp)_2]^{2+}$,[43] implying they undergo a degree of ligand exchange. All four complexes exhibit SCO in that solvent over the liquid range of CD_3CN (Figure 6). However, $\chi_M T$ for **8** does not tend towards zero at low temperatures, suggesting those solutions contain a fraction of high-spin material. That is presumably a consequence of the ligand exchange detected by NMR. Fits of the SCO equilibria for **8**-**10** were all significantly improved by accounting for a residual high-spin fraction of the sample at low temperature (Figure 6). While these corrections are estimated, the resultant fitted parameters are consistent with the other compounds in this work (Table 1), and with the DFT calculations described below.

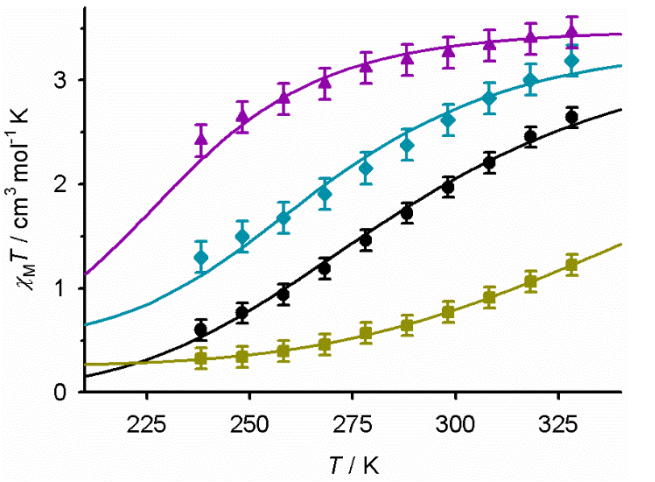

Figure 6 Magnetic data for in CD_3CN solution for **7** (black circles), **8** (yellow squares), **9** (purple triangles) and **10** (cyan diamonds). The lines show the best fits of the data to a thermodynamic SCO equilibrium. To reflect the partial ligand exchange in solution observed by NMR, the data for were fit assuming a residual low-temperature $\chi_M T$ value of 0.25 $cm^3 mol^{-1}$ K for **8**, and 0.50 $cm^3 mol^{-1}$ K for **9**-**10**.

The order in $T_{½}$ for these compounds does not perfectly mirror the corresponding trend for **3**-**6**:

9 (*L*R = L^1*i*Pr) < **10** (L^2*i*Pr) < **7** (L^1Ph) < **8** (L^2Ph)

A plot of these data for **3**-**10** shows the sterically larger *iso*propyl 'R' substituents stabilise the high-spin spin states of these complexes, compared to their phenyl-substituted congeners (Figure 7). Unexpectedly however, the spin states of **3**-**6** and **7**-**10** are very similar when *L*R = an L^1R derivative, but differ more strongly in the complexes where *L*R = L^2R. The structural basis of this difference is unclear, since crystal structures of **7**, **9** and **10** were not obtained. However the computational data below reproduce and clarify the observation, by showing the high-spin state of **8** and **10** is more stabilised than for the other $[Fe(L^2R)L]^{2+}$ complexes (Figure 7).

Gas phase DFT calculations were undertaken to shed light on these observations. The calculations were performed on **1²⁺**-**12²⁺**, the complex cations in **1**-**12**, plus the $[Fe(L^2R)(terpy)]^{2+}$ analogues of **11²⁺** and **12²⁺** (Table 2). The B86PW91 functional and def2-SVP basis set were used, to be consistent with our earlier study of $[Fe(L^1R)_2]^{2+}$ and $[Fe(L^2R)_2]^{2+}$.[30] This functional, or

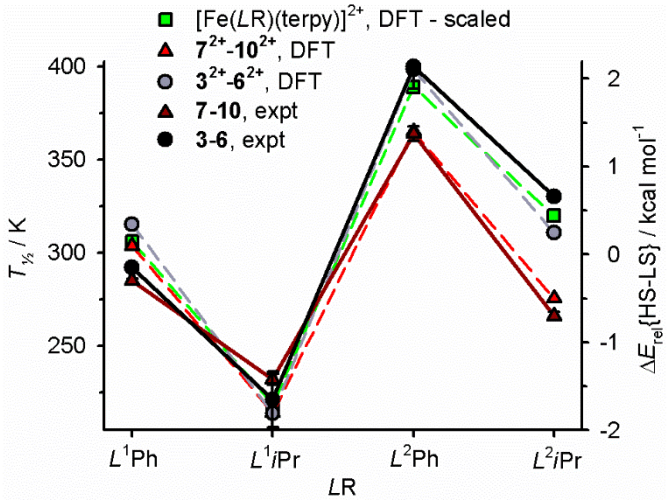

Figure 7 SCO $T_{½}$ values in solution and calculated spin state energies for the [Fe(*LR*)L][ClO$_4$]$_2$ complexes in this work. Experimental data points are linked with solid lines, while computed energies are linked with dashed lines. A constant value of 5.3 kcal mol^{-1} was subtracted from ΔE_{rel}{HS–LS} for the [Fe(*LR*)(terpy)]$^{2+}$ complexes, to bring them onto the same scale as the other molecules (Table 2). The plotted $T_{½}$ for **4** is an estimated value (experimentally >380 K).

closely related GGA functionals, with the def2-SVP basis set perform reliably in comparative studies of spin state energies, of iron(II) complexes of N-donor ligands.[30,44-46]

While only low-spin crystal structures are available, computed Fe–N distances for those molecules are consistently slightly longer than the experimental values, by up to 1.7 % (Tables S8-S9‡). That is a typical level of accuracy for a calculation of this type. As previously noted,[30] the orientation of the phenyl substituents in the minimized heteroleptic *L*^{1}Ph and *L*^{2}Ph complexes is more canted than in the crystal structures, where the bimpy or bpp ligand is sandwiched between the two *L*Ph phenyl groups (Figure S36‡). In other respects, the conformations of the molecules are well-reproduced by the calculations.

While comparison of the spin state energies in Table 2 should be reliable, their absolute values will be incorrect since pure GGA functionals like B86PW91 overstabilise the low-spin state.[47] Hence, for consistency with our previous study,[30] the energy differences between the spin states (ΔE_{rel}{HS–LS}) are scaled against [Fe(*L*^{1}H)$_2$]$^{2+}$, which shows $T_{½}$ = 245 K in solution.[28] A positive ΔE_{rel}{HS–LS} means the low-spin state is computed to be more stable than for [Fe(*L*^{1}H)$_2$]$^{2+}$, implying a higher $T_{½}$ value, while the converse is true when $T_{½}$ is negative. A plot of ΔE_{rel}{HS–LS} *vs* measured solution $T_{½}$ shows good linearity, for **1**$^{2+}$-**10**$^{2+}$ and the homoleptic complexes in ref. 30 (Figure 8). That confirms the data in Table 1 are a good description of the spin states of the complexes, despite the ligand exchange reactions observed in some cases. The sole exception is [Fe((*R*)-*L*^{2}*i*Pr)((*S*)-*L*^{2}*i*Pr)]$^{2+}$ [point (vi) in Figure 8], whose high-spin state was previously computed to be ≥1.5 kcal mol^{-1} more stable than

Table 2 Minimized gas-phase spin state energies for the complexes in this work, and their experimental solution-phase SCO mid-point temperatures ($T_{½}$; HS = high-spin, LS = low-spin). Previously published data for the homoleptic analogues of **1**$^{2+}$ and **2**$^{2+}$ are also listed, for comparison. The Roman numerals correspond to the labels in Figure 8.

		$T_{½}$, K	*E*(HS), Ha	*E*(LS), Ha	ΔE_{rel}{HS–LS}, kcal mol^{-1} [a]	ΔE{het, HS}, kcal mol^{-1} [b]	ΔE{het, LS}, kcal mol^{-1} [b]
(i)	[Fe((*S*)-*L*^{1}Ph)((*R*)-*L*^{1}Ph)]$^{2+}$ [c]	278	−3667.642858	−3667.668452	+0.1	+0.7	+2.7
(ii)	[Fe((*S*)-*L*^{1}Ph)((*R*)-*L*^{2}Ph)]$^{2+}$ (**1**$^{2+}$)	344	−4313.509676	−4313.535977	+0.6	+3.2	+3.4
(iii)	[Fe((*S*)-*L*^{2}Ph)((*R*)-*L*^{2}Ph)]$^{2+}$ [c]	LS	−4959.375037	−4959.404693	+2.7	+4.7	+4.9
(iv)	[Fe((*S*)-*L*^{1}*i*Pr)((*R*)-*L*^{1}*i*Pr)]$^{2+}$ [c]	HS	−3215.314169	−3215.333782	−3.6	+1.0	+2.3
(v)	[Fe((*S*)-*L*^{1}*i*Pr)((*R*)-*L*^{2}*i*Pr)]$^{2+}$ (**2**$^{2+}$)	241	−3861.179662	−3861.202377	−1.7	+1.3	+5.0
(vi)	[Fe((*S*)-*L*^{2}*i*Pr)((*R*)-*L*^{2}*i*Pr)]$^{2+}$ [c]	LS	−4507.046550	−4507.072196	+0.2	+2.4	+8.6
(vii)	[Fe((*R*)-*L*^{1}Ph)(bimpy)]$^{2+}$ (**3**$^{2+}$)	292	−3470.827493	−3470.853345	+0.3	+2.6	+2.5
(viii)	[Fe((*R*)-*L*^{2}Ph)(bimpy)]$^{2+}$ (**4**$^{2+}$)	>380	−4116.694033	−4116.722835	+2.1	+0.9	+2.2
(ix)	[Fe((*R*)-*L*^{1}*i*Pr)(bimpy)]$^{2+}$ (**5**$^{2+}$)	221	−3244.665626	−3244.687994	−1.9	+3.0	+5.6
(x)	[Fe((*R*)-*L*^{2}*i*Pr)(bimpy)]$^{2+}$ (**6**$^{2+}$)	330	−3890.531584	−3890.557307	+0.2	+2.1	+2.5
(xi)	[Fe((*R*)-*L*^{1}Ph)(bpp)]$^{2+}$ (**7**$^{2+}$)	285	−3163.559761	−3163.585339	+0.1	+2.9	+3.0
(xii)	[Fe((*R*)-*L*^{2}Ph)(bpp)]$^{2+}$ (**8**$^{2+}$)	364	−3809.426471	−3809.454074	+1.4	+1.3	+2.3
(xiii)	[Fe((*R*)-*L*^{1}*i*Pr)(bpp)]$^{2+}$ (**9**$^{2+}$)	232	−2937.396771	−2937.419258	−1.8	+2.7	+5.6
(xiv)	[Fe((*R*)-*L*^{2}*i*Pr)(bpp)]$^{2+}$ (**10**$^{2+}$)	266	−3583.263437	−3583.288050	−0.5	+2.2	+2.2
–	[Fe((*R*)-*L*^{1}Ph)(terpy)]$^{2+}$ (**11**$^{2+}$)	–[d]	−3207.732234	−3207.766161	+5.4	+1.6	+1.6
–	[Fe((*R*)-*L*^{2}Ph)(terpy)]$^{2+}$	–	−3853.599064	−3853.635905	+7.2	+0.1	+1.5
–	[Fe((*R*)-*L*^{1}*i*Pr)(terpy)]$^{2+}$ (**12**$^{2+}$)	–[d]	−2981.570904	−2981.601831	+3.5	+2.4	+5.3
–	[Fe((*R*)-*L*^{2}*i*Pr)(terpy)]$^{2+}$	–	−3627.436644	−3627.471112	+5.7	+1.4	+2.2

[a] A positive ΔE_{rel}{HS–LS} means the low-spin state is more stable than for [Fe(*L*^{1}H)$_2$]$^{2+}$, and *vice versa*. Spin state energies for the reference molecule [Fe(*L*^{1}H)$_2$]$^{2+}$ computed by the same method are given in Table S11‡. [b] A positive ΔE{het} means heteroleptic [Fe(*LR*)L]$^{2+}$ is more stable than an equimolar mixture of homoleptic [Fe(*LR*)$_2$]$^{2+}$ and [FeL$_2$]$^{2+}$ by this protocol. This parameter is equivalent to ΔE{dia} in ref. 30. Computed energies of homoleptic complexes used to calculate ΔE{het} are listed in Table S12‡. [c] From ref. 30. [d] While these complexes weren't isolated in pure form, preliminary NMR and magnetic data imply they are low-spin molecules (Figures S28-S32‡).[40]

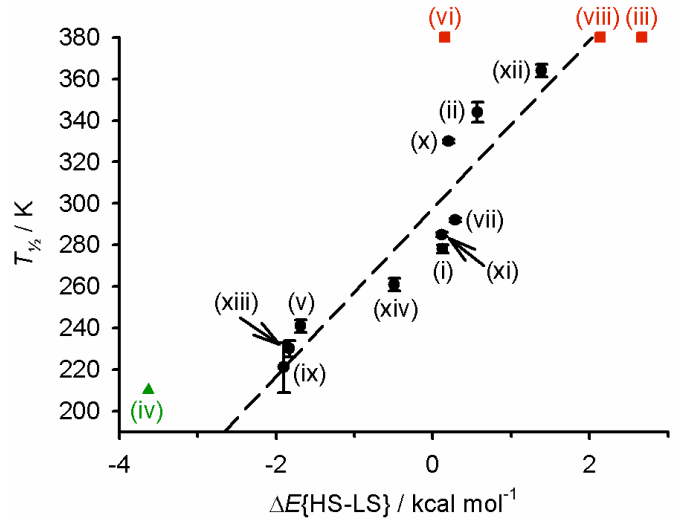

Figure 8 Correlation between measured solution $T_{½}$ values and the computed spin-state energies in Table 2. Each data point is identified by the corresponding entry in Table 2, and the line shows the best fit linear regression of the black data points. Compounds showing SCO near room temperature are black circles. Low-spin compounds ($T_{½}$ > 350 K) are red squares, and high-spin compounds ($T_{½}$ < 220 K) are green triangles.

expected by this protocol, given its experimental low-spin state.[30] Steric contacts between the *iso*propyl groups in that crowded molecule may be imperfectly modelled by our calculations, which do not include dispersion interactions between non-bonded atoms.[48,49] Interestingly, however, the energies of **2**$^{2+}$ do not show the same anomaly [point (v), Figure 8], although its minimised geometry closely resembles the homoleptic L^2*i*Pr complex.[30]

The terpy-containing complexes are not shown in Figure 8, but are computed to be low-spin (Table 2). While none of these was unambiguously isolated in pure form, preliminary data from crude **11** and **12** are consistent with that prediction (Figures S28-S32‡).[40]

As noted above, the trends in the experimental $T_{½}$ values for the [Fe(*L*R)(bimpy)]$^{2+}$ and [Fe(*L*R)(bpp)]$^{2+}$ complexes show some differences which are reproduced in the computed ΔE_{rel}{HS–LS} values. While they are consistently *ca* 5 kcal mol^{-1} more positive, the relative dependence of the spin state energies of [Fe(*L*R)(terpy)]$^{2+}$ on *L*R closely mirrors **3**$^{2+}$-**6**$^{2+}$ (Figure 7). Hence, the bpp complexes **7**$^{2+}$-**10**$^{2+}$ are apparently anomalous in this respect. This is addressed further below.

The stability of the heteroleptic complexes towards ligand exchange in the gas phase was estimated by Δ*E*{het} [eq (1)]:

$$\Delta E\{\text{het}\} = \frac{\left(E\{[\text{Fe}(L^{\text{R}})_2]^{2+}\} + E\{[\text{FeL}_2]^{2+}\}\right) - 2\left(E\{[\text{Fe}(L^{\text{R}})\text{L}]^{2+}\}\right)}{2} \quad (1)$$

All the heteroleptic complexes gave small, positive Δ*E*{het} values which computes them to be more stable than a 1:1 mixture of the corresponding homoleptic species (Table 1). A consistent trend is observed in [Fe(*L*R)L]$^{2+}$ for each 'L' ligand, with the largest Δ*E*{het} (5.3-5.6 kcal mol^{-1}) being observed when *L*R = L^1*i*Pr in the low-spin state, and the lowest Δ*E*{het} (0.1-1.3 kcal mol^{-1}) for high-spin complexes with *L*R = L^2Ph. Other molecules in the Table show values between these extremes, with Δ*E*{het} being greater for L = bimpy and bpp than when L = terpy. Δ*E*{het} is slightly larger in the low-spin state in some complexes, especially when *L*R = L^1*i*Pr, while for others it is essentially equal in both spin states.

To quantify the contribution of the phenyl and isopropyl substituents to the stability of **3**$^{2+}$-**12**$^{2+}$, Δ*E*{het} was also calculated for the corresponding unsubstituted complexes [Fe(L^1H)L]$^{2+}$ and [Fe(L^2H)L]$^{2+}$ (L = bimpy, bpp or terpy; Figure S43). These compounds show −0.3 ≤ Δ*E*{het} ≤ +1.5 kcal mol^{-1}, with Δ*E*{het} now being slightly but consistently more positive in the high-spin state (Table S12‡). Comparison of the Δ*E*{het} values in Table 2 and Table S12‡ shows the steric influence of the LR R groups increases Δ*E*{het}, by up to 5.3 kcal mol^{-1} for low-spin [Fe(L^1*i*Pr)L]$^{2+}$ and by around half that amount for the other [Fe(*L*R)L]$^{2+}$ molecules.

Discussion

Comparison of the low-spin *d*-orbital energies of the complexes highlights some differences, which are exemplified by Figure 9. Replacing L^1Ph with L^2Ph in [Fe(*L*Ph)(bpp)]$^{2+}$ leads to strengthening of the Fe–N σ-bonds (higher energies for d_{z^2} and d_{xy}, which has metal–ligand σ symmetry in the C_{2v} point group), but has little effect on their metal-ligand π-bonding. Conversely, the same comparison for [Fe(*L*Ph)(bimpy)]$^{2+}$ shows smaller differences in the Fe–N σ-bonding, but stronger metal⟶ligand π-bonding character in the L^2Ph complex (lower energies for d_{xz}, d_{yz} and $d_{x^2-y^2}$, which is metal–ligand π-bonding in C_{2v} symmetry). Similar trends are seen when the [Fe(*L*i*Pr)(bimpy)]$^{2+}$ and [Fe(*L*i*Pr)(bpp)]$^{2+}$ complexes are compared (Figures S37-S38‡), while the *d*-orbital energy trends in [Fe(L^1R)(terpy)]$^{2+}$ and [Fe(L^2R)(terpy)]$^{2+}$ broadly resemble the bimpy complexes (Figure S39‡).

All these changes increase the ligand field in each L^2R complexes compared to their L^1R congener, which stabilises their low-spin state as observed. However, the stronger metal⟶ligand π-bonding in [Fe(L^2R)L]$^{2+}$ when L is bimpy and terpy has a greater influence on the ligand field of those complexes, than the stronger metal⟵ligand σ-bonding when L = bpp. That explains why [Fe(*L*R)(bimpy)]$^{2+}$ and [Fe(*L*R)(terpy)]$^{2+}$ are more sensitive to the identity of *L*R, for a given R group.

The observations in Figure 9 can be rationalised by consideration of the metal-free ligands, which were minimised by the same protocol in the *cisoid* conformation required for metal coordination. The ligand Brønsted basicities correlate with Fe–N σ-bond strength, and were estimated from the average energies of their three lone pair combination MOs (Table S10‡):

terpy >> L^2*i*Pr ≈ bimpy > L^1*i*Pr > L^2Ph > L^1Ph > bpp

Since bpp is the least basic ligand on this list, the more basic *L*R ligands make the largest contribution to the σ-ligand field of [Fe(*L*R)(bpp)]$^{2+}$. The electronic structure of the bpp complexes should therefore be strongly influenced by the identity of *L*R. In contrast, the σ-ligand field of [Fe(*L*R)(bimpy)]$^{2+}$ and [Fe(*L*R)(terpy)]$^{2+}$ includes larger contributions from the bimpy and terpy co-ligands. Hence, changes to *L*R induce a smaller perturbation to the Fe–N σ-bonding in those molecules.

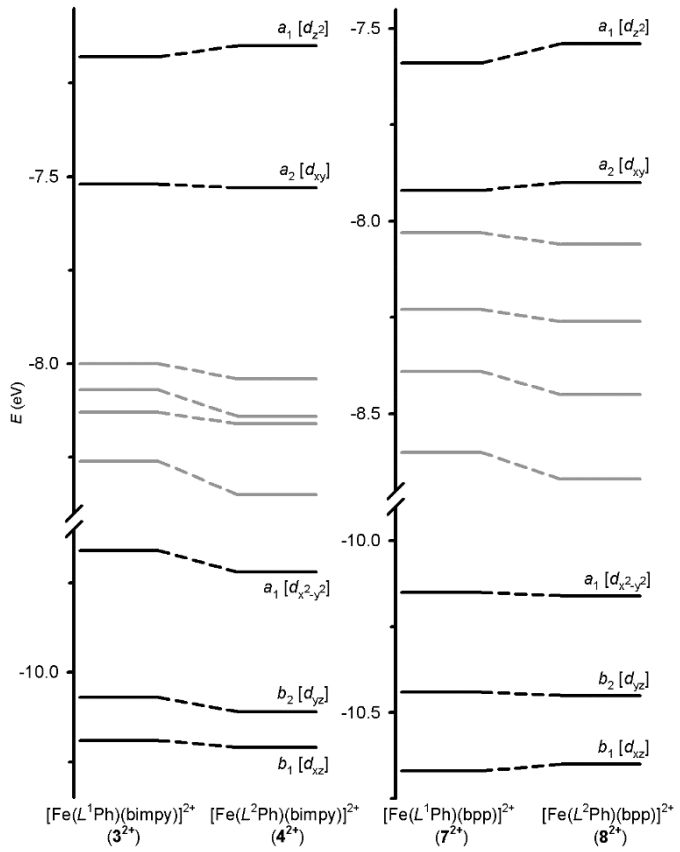

Figure 9 Computed frontier molecular orbital energies of the low-spin [Fe(*L*R)(bimpy)]$^{2+}$ and [Fe(*L*R)(bpp)]$^{2+}$ derivatives with phenyl 'R' substituents. The metal-based *d*-orbitals are shown in black, ligand-centred orbitals are de-emphasised in grey, and all the graphs are plotted with the same vertical expansion. The *d*-orbitals have C_{2v} symmetry labels, which is the point group of an idealised [Fe(*L*R)L]$^{2+}$ molecule if the 'R' substituents are discounted. Orbital plots for the other [Fe(*L*R)L]$^{2+}$ complexes are in Figures S37-S39‡.

Ranking the π-acidity of the ligands is more difficult, because both their π-donor (from the distal heterocyclic donor groups) and π-acceptor (to the central pyridyl ring) properties must be considered. However, the frontier orbitals of bpp imply it is both a worse π-donor and a worse π-acceptor than the other azolyl ligands in this study. That is, bpp has less overall metal–ligand π-bonding capability (Figure S41‡). Since *L*^{1}R and *L*^{2}R ligands with the same R group also have similar π-acidity,[30] the identity of *L*R has little effect on the π-ligand field of [Fe(*L*R)(bpp)]$^{2+}$. Conversely, the more π-acidic bimpy and terpy co-ligands should afford a softer π-ligand field in those complexes, which is more sensitive to changes elsewhere in their ligand sphere.

The π-frontier orbital energies for terpy imply it is the best π-acceptor ligand in this study (Figure S41‡). Since it contains the strongest π-donor *and* the best π-acceptor co-ligand, [Fe(*L*R)(terpy)]$^{2+}$ should be the most strongly low-spin [Fe(*L*R)L]$^{2+}$ complexes, as observed.[40]

Conclusions

Two types of heteroleptic iron(II) perchlorate complexes have been achieved, supported by PyBox (*L*^{1}R) or ThioPyBox (*L*^{2}R) ligands bearing phenyl or *iso*propyl substituents. First are heterochiral [Fe(*L*^{1}R)(*L*^{2}R)][ClO$_4$]$_2$ (R = Ph {**1**} or *i*Pr {**2**}), with *L*^{1}R and *L*^{2}R ligands of opposite chirality. The molecular structures of **1** and **2** resemble homoleptic [Fe((*R*)-*L*^{1}R)((*S*)-*L*^{1}R)][ClO$_4$]$_2$[28,29] and [Fe((*R*)-*L*^{2}R)((*S*)-*L*^{2}R)][ClO$_4$]$_2$,[30] where the comparison can be made. Their spin state properties also lie between those of the two homoleptic counterparts, in that sequential replacement of each *L*^{1}R ligand by the corresponding *L*^{2}R derivative progressively stabilises the low-spin state of the complexes (Table 1). Other heteroleptic, heterochiral [Fe(*L*^{1}R^1)(*L*^{2}R^2)]$^{2+}$ complexes bearing different substituents at each ligand (*ie* R^1 ≠ R^2) would allow their spin states to be tuned still further.

Two other families of compounds were also isolated, namely [Fe(*L*R)(bimpy)][ClO$_4$]$_2$ (**3**-**6**; *L*R = *L*^{1}Ph, *L*^{2}Ph, *L*^{1}*i*Pr or *L*^{2}*i*Pr) and [Fe(*L*R)(bpp)][ClO$_4$]$_2$ (**7**-**10**). Preliminary characterisation of some [Fe(*L*R)(terpy)][ClO$_4$]$_2$ complexes was also achieved, although these were not obtained as single-component products. Since the thermodynamic stability of [Fe(*L*R)(terpy)]$^{2+}$ towards ligand exchange resembles the other complexes (Table 2), our inability to isolate them in pure form should have a kinetic origin. Both [Fe(*L*R)(terpy)]$^{2+}$ and homoleptic [Fe(terpy)$_2$]$^{2+}$ are computed to be strongly low-spin (Tables 2 and S11), and thus very inert to ligand exchange reactions. That will inhibit equilibration of the iron/*L*R/terpy solutions towards the favoured heteroleptic product.

The low-spin forms of **3**, **4**, **6** and **8** were structurally characterised, whose *L*R 'R' substituents had no obvious steric influence on the molecular geometry. However crystals **5** have a mixed spin-state population at 120 K, which may relate to a sterically induced canting of the bimpy ligand induced by that complex's *i*Pr substituents.

While their solid state magnetic properties are unexceptional, **3**-**10** all exhibit complete or partial thermal SCO over the liquid range of CD_3CN. Some complexes show a residual high-spin population at low temperatures, which are assigned to the products of partial ligand exchange detected by ^{1}H NMR. However, in other respects the SCO equilibria appear unaffected by these solution reactions. Firstly, their $T_{½}$ values are in good agreement with their computed spin state energies (Figure 8). Secondly, the measured ΔH and ΔS values are typical for complexes of this type (Table 1),[50] and show no evidence for a ligand exchange pre-equilibrium.[51] Hence, the ligand exchange causing incomplete SCO occurs more slowly than the timescale of the NMR measurement.

Gas phase DFT calculations reproduce well the $T_{½}$ values measured in this work. The only anomaly in Figure 8, [Fe((*R*)-*L*^{2}*i*Pr)((*S*)-*L*^{2}*i*Pr)]$^{2+}$ [point (vi)], is taken from a previous study of homoleptic [Fe(*L*^{2}R)$_2$]$^{2+}$ complexes.[30] Interestingly, however, the properties of **2**$^{2+}$ are well-reproduced by our DFT protocol [point (v)]. It's unclear why replacing the two remaining O atoms in **2**$^{2+}$ by S atoms should lead to such a discrepancy. The steric properties of the *L*R 'R' groups stabilise the heteroleptic complexes by *ca* 5 kcal mol^{-1} in the low-spin state, and by 2-3 kcal mol^{-1} in their high-spin forms.

The calculations reproduce the experimental observation, that the dependence of $T_{½}$ on *L*R is different in the [Fe(*L*R)(bimpy)]$^{2+}$ (**3**$^{2+}$-**6**$^{2+}$) and [Fe(*L*R)(bpp)]$^{2+}$ (**7**$^{2+}$-**10**$^{2+}$) series (Figures 7-8). There is no simple structural explanation for this, but the calculations confirm **7**$^{2+}$-**10**$^{2+}$ show more variation in

their e_g *d*-orbital energies, but less variation in the t_{2g} subshell, than for **3**$^{2+}$-**6**$^{2+}$ or the corresponding [Fe(*L*R)(terpy)]$^{2+}$ complexes.

Further DFT calculations suggest this reflects the electronic character of the ligands used (Figure S41‡). On one hand, bpp is a weaker σ-donor and has reduced metal–ligand π-bonding character, compared to the other ligands in the study. On the other, *L*^{2}R ligands are more σ-basic than their *L*^{1}R congeners with a given R group, but have similar overall π-acidity. Hence, changing the more σ-basic *L*R ligand has a large influence on the metal–ligand σ-bonding of [Fe(*L*R)(bpp)]$^{2+}$, but has little effect on their π-ligand field. Conversely the stronger σ-ligand field in [Fe(*L*R)(bimpy)]$^{2+}$ and [Fe(*L*R)(terpy)]$^{2+}$ means changes to *L*R cause a smaller perturbation to their Fe–N σ-bonding, but the stronger π-bonding character of bimpy and terpy makes their π-ligand-field more sensitive to the rest of the ligand sphere.

To summarise, the spin states of heteroleptic iron(II) complexes of this type show a complicated dependence on the identity of the ligands present. This appears to reflect an interplay of the relative σ-basicities and π-acidities of the two ligands in each molecule.

Experimental

The *L*^{1}R,[52] *L*^{2}R[30] and bpp[53] ligands were synthesised using literature procedures. Other ligand and metal salt reagents, and organic solvents, were purchased commercially and used as supplied.

Caution. Although we have experienced no problems when using the perchlorate salts in this study, metal–organic perchlorates are potentially explosive and should be handled with care in small quantities.

Complex synthesis. The same basic protocol, with minor variations, was used to synthesise all the complexes.[37] Around 0.24 mmol of the two ligands used was dissolved in acetonitrile (20 cm^3), then an equimolar amount of solid $Fe[ClO_4]_2{\cdot}6H_2O$ was added to the solution. The mixture was stirred at room temperature for between 2-20 hrs, depending on the ligands present, then concentrated to *ca* 5 cm^3 volume. Slow diffusion of diethyl ether vapour into the filtered solution yielded the solid complex products, some of which required recrystallisation to achieve analytical purity.

Further synthetic details and characterisation data for the complexes are given in the ESI‡.

Single crystal X-ray structure analyses

All crystals were grown by slow diffusion of diethyl ether vapour into concentrated solutions of the complexes. Nitromethane was used as the crystallisation solvent for **1**$\cdot$$MeNO_2$, while all the other crystals were obtained from acetonitrile solution.

Diffraction data for **4** were collected at station I19 of the Diamond synchrotron (λ = 0.6889 Å). The other crystals were measured with an Agilent Supernova dual source diffractometer using monochromated Cu-K_α radiation (λ = 1.54184 Å). Experimental details of each structure determination, and full details of all the crystallographic refinements, are given in the ESI‡ (Table S1‡). The structures were solved by direct methods (*SHELXS*),[54] and developed by full least-squares refinement on F^2 (*SHELXL-2018*).[54] Crystallographic figures were prepared using *X-SEED*,[55] and structural parameters listed in the ESI‡ were calculated with *Olex 2*.[56]

Other measurements

Elemental microanalyses were performed by the the London Metropolitan University School of Human Sciences analytical service. Diamagnetic NMR spectra employed a Bruker AV3HD spectrometer operating at 400.1 (^{1}H) or 100.6 MHz (^{13}C), while paramagnetic ^{1}H NMR spectra were obtained with a Bruker AV3 spectrometer operating at 300.1 MHz. X-ray powder diffraction measurements were obtained at room temperature from a Bruker D2 Phaser diffractometer, using Cu-K_α radiation (λ = 1.5419 Å).

Magnetic susceptibility measurements were performed using a Quantum Design MPMS-3 VSM magnetometer, in an applied field of 5000 G with a temperature ramp of 5 K min^{-1}. Diamagnetic corrections for the samples were estimated from Pascal's constants;[57] a diamagnetic correction for the sample holder was also applied to the data. Susceptibility measurements in solution were obtained by Evans method using a Bruker AV-NEO spectrometer operating at 500.2 MHz.[58] A diamagnetic correction for the sample,[57] and a correction for the variation of the density of the CD_3CN solvent with temperature,[59] were applied to these data. Thermodynamic parameters and equilibrium midpoint temperatures ($T_{½}$) were derived by fitting these data to eq 2 and 3, where *n*HS(*T*) is the high-spin fraction of the sample at temperature *T*:

$$\ln[(1-n\mathrm{HS}(T))/n\mathrm{HS}(T)] = \Delta H/RT - \Delta S/R \quad (2)$$

$$\Delta S = \Delta H/T_{½} \quad (3)$$

Curve fitting and graph preparation were performed using *SigmaPlot*.[60]

DFT calculations were carried out using *SPARTAN*'18 for Windows,[61] with the B86PW91 functional and the def2-SVP basis set. Low-spin systems were treated as spin-restricted, and high-spin systems were treated as spin-unrestricted. The calculations were carried out in the gas phase, since a solvent gradient for iron is not implemented in *SPARTAN*'18. The molecules were constructed *de novo* in the program, then subjected to a preliminary molecular mechanics minimisation before the full DFT energy minimisation was undertaken. The chiral [Fe(*L*R)L]$^{2+}$ complexes were calculated as their (*R*) isomers.

Conflicts of interest

There are no conflicts to declare.

Acknowledgements

This work was funded by the EPSRC (EP/N509681/1) and the Leverhulme Trust (RPG-2015-095). We also thank Diamond Light Source for access to beamline I19 (MT20570), which contributed to the results presented here.

Notes and references

1 R. C. Stoufer, D. H. Busch and W. B. Hadley, *J. Am. Chem. Soc.*, 1961, **83**, 3732; R. Hogg and R. G. Wilkins, *J. Chem Soc.*, 1962, 341; A. H. Ewald, R. L. Martin, I. G. Rossj and A. H. White, *Proc. Royal Soc. London., Ser. A*, 1964, **280**, 235; E. König, *Chem. Commun.*, 1966, 61.

2 P. Gütlich, H. A. Goodwin, (eds), Spin Crossover in Transition Metal Compounds I–III: Topics in Current Chemistry, Springer-Verlag: Berlin, 2004, vols. 233–235.

3 M. A. Halcrow, (ed), Spin-crossover materials – properties and applications, John Wiley & Sons, Chichester, UK, 2013, p. 568.

4 For recent reviews of general SCO chemistry see eg J. Zarembowitch, F. Varret, A. Hauser, J. A. Real and K. Boukheddaden, *C. R. Chim.*, 2018, **21**, 1056; K. S. Kumar, Y. Bayeh, T. Gebretsadik, F. Elemo, M. Gebrezgiabher, M. Thomas and M. Ruben, *Dalton Trans.*, 2019, **48**, 15321; Z.-S. Yao, Z. Tang and J. Tao, *Chem. Commun.*, 2020, **56**, 2071; P. Guionneau, M. Marchivie and G. Chastanet, *Chem. – Eur. J.*, 2021, **27**, 1483; W. Huang, X. Ma, O. Sato and D. Wu, *Chem. Soc. Rev.*, 2021, **50**, 6832.

5 O. Kahn, J. Kröber and C. Jay, *Adv. Mater.*, 1992, **4**, 718.

6 Recent reviews of SCO nanoscience: K. S. Kumar and M. Ruben, *Coord. Chem. Rev.*, 2017, 346, 176; S. Rat, M. Piedrahita-Bello, L. Salmon, G. Molnár, P. Demont and A. Bousseksou, *Adv. Mater.*, 2018, **30**, 1703862; E. Coronado, *Nat. Rev. Mater.*, 2020, **5**, 87; L. Kipgen, M. Bernien, F. Tuczek and W. Kuch, *Adv. Mater.*, 2021, **33**, 2008141 and 2021, **33**, 2170354 (correction).

7 For other prototype applications of SCO materials see *eg* O. I. Kucheriv, V. V. Oliynyk, V. V. Zagorodnii, V. L. Launets and I. A. Gural'skiy, *Sci. Rep.*, 2016, **6**, 38334; M. D. Manrique-Juárez, F. Mathieu, A. Laborde, S. Rat, V. Shalabaeva, P. Demont, O. Thomas, L. Salmon, T. Leichle, L. Nicu, G. Molnár and A. Bousseksou, *Adv. Funct. Mater.*, 2018, **28**, 1801970; S. P. Vallone, A. N. Tantillo, A. M. dos Santos, J. Molaison, R. Kulmaczewski, A. Chapoy, P. Ahmadi, M. A. Halcrow and K. G. Sandeman, *Adv. Mater.*, 2019, **31**, 1807334; M. Piedrahita-Bello, J. E. Angulo-Cervera, R. Courson, G. Molnár, L. Malaquin, C. Thibault, B. Tondu, L. Salmon and A. Bousseksou, *J. Mater. Chem. C*, 2020, **8**, 6001; K. Ridier, Y. Zhang, M. Piedrahita-Bello, C. M. Quintero, L. Salmon, G. Molnár, C. Bergaud and A. Bousseksou, *Adv. Mater.*, 2020, **32**, 2000987.

8 M. A. Halcrow, *Polyhedron*, 2007, **26**, 3523.

9 O. Roubeau, *Chem. – Eur. J.*, 2012, **18**, 15230.

10 N. F. Sciortino and S. M. Neville, *Aust. J. Chem.*, 2014, **67**, 1553; Z.-P. Ni, J.-L. Liu, M. N. Hoque, W. Liu, J.-Y. Li, Y.-C. Chen and M.-L. Tong, *Coord. Chem. Rev.*, 2017, **335**, 28; R. Ohtani and S. Hayami, *Chem. – Eur. J.*, 2017, **23**, 2236; O. I. Kucheriv, I. O. Fritsky and I. A. Gural'skiy, *Inorg. Chim. Acta*, 2021, **521**, 120303.

11 P. Guionneau, M. Marchivie, G. Bravic, J.-F. Létard and D. Chasseau, *Top. Curr. Chem.*, 2004, **234**, 97.

12 J. A. Kitchen and S. Brooker, *Coord. Chem. Rev.*, 2008, **252**, 2072; H. L. C. Feltham, A. S. Barltrop and S. Brooker, *Coord. Chem. Rev.*, 2017, **344**, 26.

13 H. S. Scott, R. W. Staniland and P. E. Kruger, *Coord. Chem. Rev.*, 2018, **362**, 24.

14 H. A. Goodwin, *Top. Curr. Chem.*, 2004, **233**, 59.

15 J. Olguin and S. Brooker, *Coord. Chem. Rev.*, 2011, **255**, 203.

16 G. J. Long, F. Grandjean and D. L. Reger, *Top. Curr. Chem.*, 2004, **233**, 91.

17 M. A. Halcrow, *Coord. Chem. Rev.*, 2009, **253**, 2493; L. J. Kershaw Cook, R. Mohammed, G. Sherborne, T. D. Roberts, S. Alvarez and M. A. Halcrow, *Coord. Chem. Rev.*, 2015, **289–290**, 2.

18 G. A. Craig, O. Roubeau and G. Aromí, *Coord. Chem. Rev.*, 2014, **269**, 13.

19 M. Boča, R. F. Jameson and W. Linert, *Coord. Chem. Rev.*, 2011, **255**, 290.

20 C. Provent, G. Bernardinelli, A. F. Williams and N. Vulliermet, *Eur. J. Inorg. Chem.*, 2001, 1963; S. Saaby, K. Nakama, M. A. Lie, R. G. Hazell and K. A. Jørgensen, *Chem. – Eur. J.*, 2003, **9**, 6145; H. Sato, Y. Suzuki, Y. Takai, H. Kawasaki, R. Arakawa, M. Shizuma, *Chem. Lett.*, 2010, **39**, 564; K. E. Burrows, R. Kulmaczewski, O. Cespedes, S. A. Barrett and M. A. Halcrow, *Polyhedron*, 2018, **149**, 134.

21 Y. Pankratova, D. Aleshin, I. Nikovskiy, V. Novikov and Y. Nelyubina, *Inorg. Chem.*, 2020, **59**, 7700.

22 L. A. Barrios, C. Bartual-Murgui, E. Peyrecave-Lleixà, B. Le Guennic, S. J. Teat, O. Roubeau and G. Aromí, *Inorg. Chem.*, 2016, **55**, 4110.

23 J. S. Costa, S. Rodríguez-Jiménez, G. A. Craig, B. Barth, C. M. Beavers, S. J. Teat and G. Aromí, *J. Am. Chem. Soc.*, 2014, **136**, 3869; C. Bartual-Murgui, R. Diego, S. Vela, S. J. Teat, O. Roubeau and G. Aromí, *Inorg. Chem.*, 2018, **57**, 11019; V. García-López, M. Palacios-Corella, V. Gironés-Pérez, C. Bartual-Murgui, J. A. Real, E. Pellegrin, J. Herrero-Martín, G. Aromí, M. Clemente-León and E. Coronado, *Inorg. Chem.*, 2019, **58**, 12199.

24 B. Moubaraki, B. A. Leita, G. J. Halder, S. R. Batten, P. Jensen, J. P. Smith, J. D. Cashion, C. J. Kepert, J.-F. Létard and K. S. Murray, *Dalton Trans.*, 2007, 4413; C. J. Schneider, B. Moubaraki, J. D. Cashion, D. R. Turner, B. A. Leita, S. R. Batten and K. S. Murray, *Dalton Trans.*, 2011, **40**, 6939; W. Phonsri, B. A. I. Lewis, G. N. L. Jameson and K. S. Murray, *Chem. Commun.,* 2019, **55**, 14031.

25 Several neutral, heteroleptic iron(III) complexes of dianionic and monoanionic tridentate Schiff bases have been reported, which may be stabilised against ligand exchange on electroneutrality grounds. See *eg* W. Phonsri, V. Martinez, G. N. L. Jameson, B. Moubaraki and K. S. Murray, *Chem. Commun.,* 2016, **52**, 1443; W. Phonsri, C. G. Davies, G. N. L. Jameson, B. Moubaraki and K. S. Murray, *Chem. – Eur. J.*, 2016, **22**, 1322; R. Busch, A. B. Carter, K. F. Konidaris, I. A. Kehne, R. González, C. E. Anson and A. K. Powell, *Chem. – Eur. J.*, 2020, **26**, 11835; A. Miyawaki, T. Mochida, T. Sakurai, H. Ohta and K. Takahashi, *Inorg. Chem.*, 2020, **59**, 12295; A. Miyawaki, K. Eda, T. Mochida, T. Sakurai, H. Ohta, T. Nakajima and K. Takahashi, *Inorg. Chem.*, 2021, **60**, 12735.

26 Heteroleptic SCO iron complexes can also be prepared cleanly using one tetradentate and one bidentate ligand to form an octahedral geometry. See *eg* A. J. Simaan, M.-L. Boillot, E. Rivière, A. Boussac and J.-J. Girerd, *Angew. Chem. Int. Ed.*, 2000, **39**, 196; G. S. Matouzenko, J.-F. Létard, S. Lecocq, A. Bousseksou, L. Capes, L. Salmon, M. Perrin, O. Kahn and A. Collet, *Eur. J. Inorg. Chem.*, 2001, 2935; G. S. Matouzenko, A. Bousseksou, S. A. Borshch, M. Perrin, S. Zein, L. Salmon, G. Molnar and S. Lecocq, *Inorg. Chem.*, 2004, **43**, 227; H. V. Phan, P. Chakraborty, M. Chen, Y. M. Calm, K. Kovnir, L. K. Keniley jr, J. M. Hoyt, E. S. Knowles, C. Besnard, M. W. Meisel, A. Hauser, C. Achim and M. Shatruk, *Chem. Eur. J.*, 2012, **18**, 15805; M. Schmitz, M. Seibel, H. Kelm, S. Demeshko, F. Meyer and H.-J. Krüger, *Angew. Chem. Int. Ed.*, 2014, **53**, 5988; S. Yergeshbayeva, J. J. Hrudka, J. Lengyel, R. Erkasov, S. A. Stoian, A. Dragulescu-Andrasi and M. Shatruk, *Inorg. Chem.*, 2017, **56**, 11096.

27 G. Desimoni, G. Faita and P. Quadrelli*, Chem. Rev.*, 2003, **103**, 3119; R. Connon, B. Roche, B. V. Rokade and P. J. Guiry, *Chem. Rev.*, 2021, **121**, 6373.

28 K. E. Burrows, S. E. McGrath, R. Kulmaczewski, O. Cespedes, S. A. Barrett and M. A. Halcrow, *Chem. – Eur. J.*, 2017, **23**, 9067.

29 W.-Q. Gao, Y.-S. Meng, C.-H. Liu, Y. Pan, T. Liu and Y.-Y. Zhu, *Dalton Trans.*, 2019, **48**, 6323; R.-G. Wang, Y.-S. Meng, F.-F. Gao, W.-Q. Gao, C.-H. Liu, A. Li, T. Liu and Y.-Y. Zhu, *Dalton Trans.*, 2021, **50**, 3369.

30 N. Shahid, K. E. Burrows, C. M. Pask, O. Cespedes, M. J. Howard, P. C. McGowan and M. A. Halcrow, *Inorg. Chem.*, 2021, **60**, 14336. Note that paper and this one use different systems of L^1R and L^2R ligand abbreviations.
31 Sato *et al* have used a similar strategy to prepare crystals with switchable dielectric properties, from heterometallic complexes whose metal ion sites are stabilised by opposite enantiomers of a chiral macrocyclic ligand. S. Kanegawa, Y. Shiota, S. Kang, K. Takahashi, H. Okajima, A. Sakamoto, T. Iwata, H. Kandori, K. Yoshizawa and O. Sato, *J. Am. Chem. Soc.*, 2016, **138**, 14170; P. Sadhukhan, S.-Q. Wu, J. I. Long, T. Nakanishi, S. Kanegawa, K. Gao, K. Yamamoto, H. Okajima, A. Sakamoto, M. L. Baker, T. Kroll, D. Sokaras, A. Okazawa, N. Kojima, Y. Shiota, K. Yoshizawa and O. Sato, *Nat. Commun.*, 2021, **12**, 4836.
32 See *eg* T. Hashibe, T. Fujinam, D. Furusho, N. Matsumoto and Y. Sunatsuki, *Inorg. Chim. Acta*, 2011, **375**, 338; D.-H. Ren, D. Qiu, C.-Y. Pang, Z. Li and Z.-G. Gu, *Chem. Commun.*, 2015, **51**, 788; L.-F. Qin, C.-Y. Pang, W.-K. Han, F.-L. Zhang, L. Tian, Z.-G. Gu, X. Ren and Z. Li, *Dalton Trans.*, 2016, **45**, 7340; Q. Wang, S. Venneri, N. Zarrabi, H. Wang, C. Desplanches, J.-F. Létard, T. Seda and M. Pilkington, *Dalton Trans.*, 2015, **44**, 6711; Y. Sekimoto, M. R. Karim, N. Saigo, R. Ohtani, M. Nakamura and S. Hayami, *Eur. J. Inorg. Chem.*, 2017, 1049; C. Bartual-Murgui, L. Piñeiro-López, F. J. Valverde-Muñoz, M. C. Muñoz, M. Seredyuk and J. A. Real, *Inorg. Chem.*, 2017, **56**, 13535; V. B. Jakobsen, L. O'Brien, G. Novitchi, H. Müller-Bunz, A.-L. Barra and G. G. Morgan, *Eur. J. Inorg. Chem.*, 2019, 4405; T.-T. Ma, X.-P. Sun, Z.-S. Yao and J. Tao, *Inorg. Chem. Front.*, 2020, **7**, 1196.
33 V. Jornet-Mollá, Y. Duan, C. Giménez-Saiz, Y.-Y. Tang, P.-F. Li, F. M. Romero and R.-G. Xiong, *Angew. Chem. Int. Ed.*, 2017, **56**, 14052; R. Akiyoshi, Y. Hirota, D. Kosumi, M. Tsutsumi, M. Nakamura, L. F. Lindoy and S. Hayami, *Chem. Sci.*, 2019, **10**, 5843; R. Akiyoshi, Y. Komatsumaru, M. Donoshita, S. Dekura, Y. Yoshida, H. Kitagawa, Y. Kitagawa, L. F. Lindoy and S. Hayami, *Angew. Chem. Int. Ed.*, 2021, **60**, 12717.
34 S. Ohkoshi, S. Takano, K. Imoto, M. Yoshikiyo, A. Namai and H. Tokoro, *Nat. Photonics*, 2014, **8**, 65.
35 Other homoleptic $[Fe(L^1R)_2]^{2+}$ complex derivatives: Y.-Y. Zhu, H.-Q. Li, Z.-Y. Ding, X.-J. Lü, L. Zhao, Y.-S. Meng, T. Liu and S. Gao, *Inorg. Chem. Front.*, 2016, **3**, 1624; A. Kimura and T. Ishida, *Inorganics*, 2017, **5**, 52; B.-X. Luo, Y. Pan, Y.-S. Meng, Q. Liu, J. Yin, T. Liu and Y.-Y. Zhu, *Eur. J. Inorg. Chem.*, 2021, 3992.
36 Other homoleptic $[Fe(L^2R)_2]^{2+}$ complexes: J. D. Nobbs, A. K. Tomov, R. Cariou, V. C. Gibson, A. J. P. White and G. J. P. Britovsek, *Dalton Trans.*, 2012, **41**, 5949; Y. Pan, Y.-S. Meng, Q. Liu, W.-Q. Gao, C.-H. Liu, T. Liu and Y.-Y. Zhu, *Inorg. Chem.*, 2020, **59**, 7398.
37 Our use of (*R*) or (*S*) enantiomer L^1R and L^2R ligands in each complex was governed by the availability of those ligands in the laboratory. Supplies of L^2iPr were particularly limited, since its synthesis is low-yielding and involves a difficult purification.[30]
38 J. Elhaïk, D. J. Evans, C. A. Kilner and M. A. Halcrow, *Dalton Trans.*, 2005, 1693.
39 C. M. Harris, H. R. H. Patil and E. Sinn, *Inorg. Chem.*, 1969, **8**, 101.
40 ^{1}H NMR spectra of **11** and **12** contain multiple diamagnetic species, with a small quantity of paramagnetic $[Fe((R)\text{-}L^1i\text{Pr})_2]^{2+}$ [28] also present in solutions of **12** (Figure S31‡). These solutions are diamagnetic (**11**), or have a small, constant paramagnetism (**12**), by Evans method (Figure S32‡). Assuming intact **11** and **12** are present in those solutions, that implies those complexes are diamagnetic and low-spin as predicted by the DFT calculations (Table 2).
41 See *e.g.* M. Clemente-León, E. Coronado, M. C. Giménez-López and F. M. Romero, *Inorg. Chem.*, 2007, **46**, 11266; J. J. M. Amoore, S. M. Neville, B. Moubaraki, S. S. Iremonger, K. S. Murray, J.-F. Létard and C. J. Kepert, *Chem. – Eur. J.*, 2010, **16**, 1973; T. D. Roberts, F. Tuna, T. L. Malkin, C. A. Kilner and M. A. Halcrow, *Chem. Sci.*, 2012, **3**, 349; W. Phonsri, C. G. Davies, G. N. L. Jameson, B. Moubaraki and K. S. Murray, *Chem. – Eur. J.*, 2016, **22**, 1322; R. G. Miller and S. Brooker, *Chem. Sci.*, 2016, **7**, 2501; C. Bartual-Murgui, C. Codina, O. Roubeau and G. Aromí, *Chem. – Eur. J.*, 2016, **22**, 12767; J. E. Clements, P. R. Airey, F. Ragon, V. Shang, C. J. Kepert and S. M. Neville, *Inorg. Chem.*, 2018, **57**, 14930; N. Li, J.-P. Xue, J.-L. Liu, Y.-Y. Wang, Z.-S. Yao and J. Tao, *Dalton Trans.*, 2020, **49**, 998; I. Capel Berdiell, R. Kulmaczewski, N. Shahid, O. Cespedes and M. A. Halcrow, *Chem. Commun.*, 2021, **57**, 6566; F.-L. Yang, W.-H. Wu, Y.-Q. Wang, X. Chen, B.-B. Liang, H.-L. Mi, G.-L. Zhang, X.-Y. Chen and Y. Shi, *Cryst. Growth Des.*, 2021, **21**, 6671.
42 See e.g.: G. Ritter, E. König, W. Irler and H. A. Goodwin, *Inorg. Chem.*, 1978, **17**, 224; Y. Garcia, V. Ksenofontov, S. Mentior, M. Dirtu, C. Gieck, A. Bhatthacharjee and P. Gütlich, *Chem. – Eur. J.*, 2008, **14**, 3745; J.-F. Létard, S. Asthana, H. J. Shepherd, P. Guionneau, A. E. Goeta, N. Suemura, R. Ishikawa and S. Kaizaki, *Chem. – Eur. J.*, 2012, **18**, 5924; R. Kulmaczewski, E. Trzop, L. J. Kershaw Cook, E. Collet, G. Chastanet and M. A. Halcrow, *Chem. Commun.*, 2017, **53**, 13268; Y. S. Ye, X. Q. Chen, Y. D. Cai, B. Fei, P. Dechambenoit, M. Rouzières, C. Mathonière, R. Clérac and X. Bao, *Angew. Chem. Int. Ed.*, 2019, **58**, 18888; M. Książek, M. Weselski, M. Kaźmierczak, A. Tołoczko, M. Siczek, P. Durlak, J. A. Wolny, V. Schünemann, J. Kusz and R. Bronisz, *Chem. – Eur. J.*, 2020, **26**, 14419.
43 J. M. Holland, J. A. McAllister, C. A. Kilner, M. Thornton-Pett, A. J. Bridgeman and M. A. Halcrow, *J. Chem. Soc. Dalton Trans.*, 2002, 548.
44 I. Capel Berdiell, R. Kulmaczewski and M. A. Halcrow, *Inorg. Chem.*, 2017, **56**, 8817; R. Kulmaczewski, M. J. Howard and M. A. Halcrow, *Dalton Trans.*, 2021, **50**, 3464; I. Capel Berdiell, D. J. Davies, J. Woodworth, R. Kulmaczewski, O. Cespedes and M. A. Halcrow, *Inorg. Chem.*, 2021, **60**, 14988.
45 B. J. Houghton and R. J. Deeth, *Eur. J. Inorg. Chem.*, 2014, 4573; S. R. Mortensen and K. P. Kepp, *J. Phys. Chem. A*, 2015, **119**, 4041.
46 L. J. Kershaw Cook, R. Kulmaczewski, R. Mohammed, S. Dudley, S. A. Barrett, M. A. Little, R. J. Deeth and M. A. Halcrow, *Angew. Chem., Int. Ed.*, 2016, **55**, 4327.
47 M. Reiher, O. Salomon and B. A. Hess, *Theor. Chem. Acc.*, 2001, **107**, 48; S. Zein, S. A. Borshch, P. Fleurat-Lessard, M. E. Casida and H. Chermette, *J. Chem. Phys.*, 2007, **126**, 014105.
48 An attempt to include dispersion into the calculations in ref. 30 gave much poorer agreement with experiment, than the protocol used in this study. Common functionals including dispersion corrections often over-estimate intramolecular dispersion in gas phase calculations, and strongly over-stabilise the low-spin state.[49]
49 D. C. Ashley and E. Jakubikova, *Coord. Chem. Rev.*, 2017, **337**, 97.
50 See *eg* W. Linert, M. Konecny and F. Renz, *J. Chem. Soc. Dalton Trans.*, 1994, 1523; L. J. Kershaw Cook, R. Kulmaczewski, R. Mohammed, S. Dudley, S. A. Barrett, M. A. Little, R. J. Deeth and M. A. Halcrow, *Angew. Chem. Int. Ed.*, 2016, **55**, 4327; I. Nikovskiy, A. Polezhaev, V. Novikov, D. Aleshin, A. Pavlov, E. Saffiulina, R. Aysin, P. Dorovatovskii, L. Nodaraki, F. Tuna and Y. Nelyubina, *Chem. – Eur. J.*, 2020, **26**, 5629; I. Capel Berdiell, V. García-López, M. J. Howard, M. Clemente-León and M. A. Halcrow, *Dalton Trans.*, 2021, **50**, 7417.
51 N. Hassan, A. B. Koudriavtsev and W. Linert, *Pure Appl. Chem.*, 2008, **80**, 1281; S. A. Barrett, C. A. Kilner and M. A. Halcrow, *Dalton Trans.*, 2011, **40**, 12021.
52 M. K. Tse, S. Bhor, M. Klawonn, G. Anilkumar, H. Jiao, C. Döbler, A. Spannenberg, W. Mägerlein, H. Hugl and M. Beller, *Chem. – Eur. J.*, 2006, **12**, 1855.
53 D. L. Jameson and K. A. Goldsby, *J. Org. Chem.*, 1990, **55**, 4992.

54 G. M. Sheldrick, *Acta Cryst. Sect. C: Struct. Chem.*, 2015, **71**, 3.
55 L. J. Barbour *J. Appl. Cryst.*, 2020, **53**, 1141.
56 O. V. Dolomanov, L. J. Bourhis, R. J. Gildea, J. A. K. Howard and H. Puschmann, *J. Appl. Cryst.*, 2009, **42**, 339.
57 C. J. O'Connor, *Prog. Inorg. Chem.*, 1982, **29**, 203.
58 D. F. Evans, *J. Chem. Soc.*, 1959, 2003; E. M. Schubert, *J. Chem. Educ.*, 1992, **69**, 62.
59 B. Garcia and J. C. Ortega, *J. Chem. Eng. Data*, 1988, **33**, 200.
60 *SIGMAPLOT*, v. 8.02, SPSS Scientific Inc., Chicago IL, USA, 2002.
61 *Spartan'18*, Wavefunction Inc., Irvine CA, USA, 2018.